JETIR.ORG ISSN: 2349-5162 | ESTD Year : 2014 | Monthly Issue
JOURNAL OF EMERGING TECHNOLOGIES AND INNOVATIVE RESEARCH (JETIR)
An International Scholarly Open Access, Peer-reviewed, Refereed Journal

Design and Analysis of Hybrid Energy management for Non-Integer Control with three phase Fault topology

[1] .Tupsoundar Mahendra Khanderao , 2Prof. K. Chandra Obula Reddy , 3 Prof. Uddhav G.Takle,
[1]Mtech Electrical Power System, [2]Assistant Professor,HOD [3] Prof, Department of Electrical Engineering
[1]M.S.S College of Engineering, Jalna, India

ABSTRACT:

For a grid-connected smart DC-microgrid, this research proposes an intelligent energy management controller based on a combination of fuzzy logic and fractional-order proportional-integral-derivative (FO-PID) controller approaches. It is possible to maintain power supply and sell electricity by connecting a dc micro grid to the main grid. A battery bank, wind energy, and photovoltaic (PV) energy source are among the hybrid energy sources integrated into the DC-microgrid. The new intelligent fractional order PID approach controls the source-side converters (SSCs) to harvest the greatest power from renewable energy sources (wind and PV) and improve the power quality provided to the DC-microgrid. The (wind and PV) energy sources are prioritized to make the microgrid as cost-effective as possible. The suggested controller ensures that output power is steady and that service is uninterrupted. Analyze symmetrical and asymmetrical grid fault simulation results. The proposed control's simulation results in Matlab/Simulink are shown.

Keywords: Solar PV, Wind, Battery Energy storage system, Boost Converter, Rectifier, Inverter, LC Filter, Permanent magnet synchronous generator.

I. INTRODUCTION:

The worldwide production of electrical energy results in pollution of many different kinds. The combustion of fossil fuels results in atmospheric emissions, which are caused by thermal power plants (coal, oil). However, nuclear power plants, whose construction accelerated in the wake of the oil crisis, have not had a detrimental effect on air quality. However, they also produce radioactive waste, which is extremely difficult to store, process, and transport.Renewable energies (hydraulic, wind, solar, biomass, etc.) now play a significant role in the production of electricity due to the fear of using a single energy source with all of its risks and the opening up of the electricity production market [1], [2].Consumer demand for energy is typically not distributed over time equally, which causes issues with the phasing of energy produced versus energy consumed. Production and consumption must be balanced for the grid to be stable [3]. As a result, the increase in the penetration rate of renewable energies will depend on their involvement in these various services, which will be aided by their collaboration with electrical energy storage systems [4].Therefore, storage is essential for the integration of these energies into the electrical grid. It not only gives the grid operator a technical way to guarantee a real-time balance between production and consumption, but it also makes it possible to use renewable resources as effectively as possible by preventing load shedding in the event of excess production. Decentralized storage would also have the benefit of increasing the robustness of the electricity network by enabling islanding of the area supplied by this resource when combined with local renewable generation.Additionally, a properly placed energy storage system (ESS) improves the quality of the power supplied by offering better frequency and voltage control and lessens the impact of its variability by enhancing the supplied current [5], [6]. This is especially true if the electricity is delivered during peak hours.An emerging research area is the integration of renewable energies with an energy storage system in a standalone micro grid. In general, integrating various renewable energies like tidal, wind, and solar energy is preferred because it increases the energy storage system's maximum capacity. ESS is typically made up of a battery and supercapacitors, which helps to increase battery life and provides a quick system response to

compensate for transients [7].The AC grid is used in place of supercapacitors because loads are required when all (energy sources and battery storage systems (BSS)) are connected [8]. A micro grid can be either DC, AC, or a hybrid of the two. The advantages of a DC microgrid over an AC one include simpler structure, easier integration, and fewer controllable parameters. Contrarily, AC type requires more data, such as the synchronization of the frequency and reactive power, which makes the control design process a difficult task. Furthermore, a DC micro grid provides the option to operate in a variety of ways, including standalone or integrated with an AC microgrid [9], [10].The autonomous DC microgrid can operate at its peak efficiency thanks to the most recent advancements in power electronics. However, due to the stochastic nature of renewable energy sources, an additional energy management unit is required for a smooth operation and continuous power transmission to the loads. There have been a lot of studies done on energy management control for AC microgrids, but due to the significant dynamics differences between AC and DC microgrids, these control strategies cannot be used for DC microgrids.In fact, where energy is consumed or supplied through the DC-link, the load converters and the energy sources are connected in parallel in the DC microgrid's standard design. For the DC microgrid to operate effectively and steadily, the DC-link voltage must be controlled [11], [12]. To address the problems with the DC-link voltage, a number of control strategies have been reported in the literature. A review of current developments and trends in hybrid micro grid topology with energy resource planning and control is provided in [13]. [14]Proposes a combined fuzzy controller and voltage control to control DC voltage.A fuzzy logic control strategy with fewer rules is examined in [15]. A dual proportional-integral controller is utilized in [16]. The aforementioned linear control strategies can, however, regulate the DC-link in a condensed operating interval. This paper evaluates the performance of the proposed system before and after the occurrence of fault. Section-I depicts about the introduction and literature review of the existing system. Section-II explains about the description of the system. Section-III describes about the proposed fault injected system. Section-IV depicts about results and discussion. Section-V ends with conclusion of this work.

II. DESCRIPTION OF THE SYSTEM:

Figure 1 shows the studied hybrid energy system integrated smart DC-microgrid, which is divided into three main components: the hybrid energy sources, which are made up of the wind, solar, and battery storage systems connected to the DC-link through their respective converters.In order to force the wind and solar (PV) conversion systems to operate at maximum power, a maximum power point tracking algorithm is

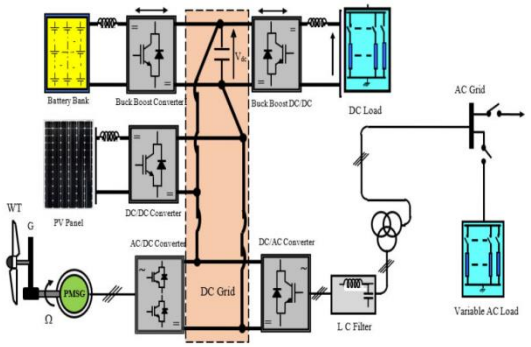

used. To choose the appropriate control modes, the energy management unit computes the total energy produced and consumed.

Figure 1: Structure of grid connected Wind-Solar PV-BES System

A. Modelling of the Wind System:

The following gives the mathematical formula for the wind energy that a turbine can convert is as:

$$\mathbf{P_m} = \frac{\mathbf{1}}{\mathbf{2}}\boldsymbol{\rho}\mathbf{C_p}(\boldsymbol{\beta},\boldsymbol{\lambda})\mathbf{A}\mathbf{V}^{\mathbf{3}} \ (\mathbf{1})$$

$$\boldsymbol{T_m} = \frac{\boldsymbol{P_m}}{\boldsymbol{\omega_t}} \ (\mathbf{2})$$

$$\boldsymbol{C_p}(\boldsymbol{\beta},\boldsymbol{\lambda}) = \frac{\mathbf{1}}{\mathbf{2}}\left(\frac{\mathbf{116}}{\boldsymbol{\lambda_i}} - \mathbf{0.4}\boldsymbol{\beta} - \mathbf{5}\right)\boldsymbol{e}^{-\left(\frac{\mathbf{21}}{\boldsymbol{\lambda_i}}\right)} \qquad (\mathbf{3})$$

Where v is the wind speed, is the pitch angle, t is the turbine speed, R is the radius of the blades, Cp is the power coefficient, λ is the tip-speed ratio,ρ is the water density, and A is the area of the blades. The permanent magnet synchronous generator (PSMG), which is the foundation of the wind conversion system, is described as

$$\boldsymbol{V_{dq}} = \boldsymbol{R_{dq}}\boldsymbol{I_{dq}} + \boldsymbol{L_{dq}}\boldsymbol{I_{dq}} + \boldsymbol{\psi_{dq}}\boldsymbol{p}\boldsymbol{w_m} \qquad (\mathbf{4})$$

Where, $\boldsymbol{i_{dq}} = \begin{bmatrix}\boldsymbol{i_d}\\ \boldsymbol{i_q}\end{bmatrix}$signifies the current vector of the stator, the electromagnetic torque is represented by Te, the viscous friction coefficient is represented by ffv, $L_{dq} = \begin{bmatrix}L_d & 0\\ 0 & L_q\end{bmatrix}$J is the moment of inertia, and represents the dq inductances matrix $\psi_{dq} = \begin{bmatrix}\psi_f\\ 0\end{bmatrix}$represents the vector of flux linkages, $V_{dq} = \begin{bmatrix}V_d\\ V_q\end{bmatrix}$demonstrates the voltage stator vector,and $L_{dq} = \begin{bmatrix}R_s & 0\\ 0 & R_s\end{bmatrix}$represents the resistance matrix of the stator.

The model of the SCCs must be expressed in order to design the suggested control method. As a result, the model of the wind source converter is presented as:

$$\frac{dV_w}{dt} = \frac{I_W}{I_C} - \frac{I_{LW}}{C_W} \text{(5)}$$

Where Iw stands for wind current rectified, Ll for inductance, ILw for inductor current, and Vw for input voltage rectifiedLink voltage is indicated by Vdc, while dynamics uncertainty in the energy stage parameters is indicated by D1 and D2. The wind system can be operated under MPPT for maximum power extraction or off-MPPT for power balance, as shown in Fig. 2, depending on the state of the storage system, which will be discussed in the energy management section. The flowchart in Fig. 3 describes the MPPT algorithm in detail.

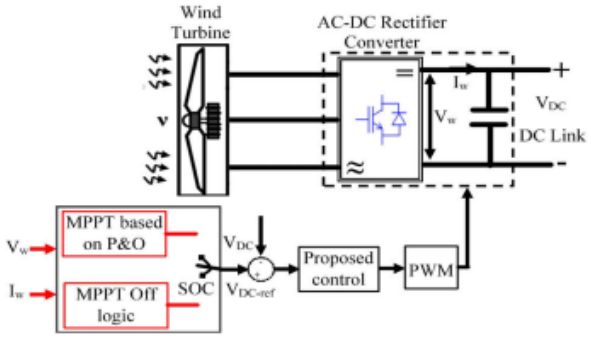

FIGURE 2. Wind energy system with controller

The proposed energy management unit (EMU) switches the wind controller from the MPPT mode to the off-MPPT mode in order to reduce the generated power and maintain a balanced power in the standalone system in the event of excess power generation and no storage capacity in the battery system. The voltage reference in off-MPPT is implemented as

$$V_{ref} = \frac{P_L - P_W}{I_W} \text{(6)}$$

Where Pw is the power from the wind energy system and PL is the load power.

B. Modelling of Solar PV:

The PV panel is connected to the DC-link through a DC-DC boost converter to form the solar conversion system (SCS). Below is the mathematical representation of the SCS.

$$\frac{dV_{PV}}{dt} = \frac{I_{PV}}{C_{PV}} - \frac{I_{LPV}}{C_{PV}} \text{(7)}$$

$$\frac{V_{PV}}{L_{PV}} = \frac{dI_{PV}}{dt} + (1 - U_2)\frac{V_{dc}}{L_{PV}} - D_3 \text{ (8)}$$

Where Ipv stands for photovoltaic current, Lpv for inductance, Vpv for photovoltaic panel voltage, LLpv for inductor current, U2 for control signal, and D3 and D4 for dynamics uncertainty in the energy stage parameters, as shown in Figure 3.

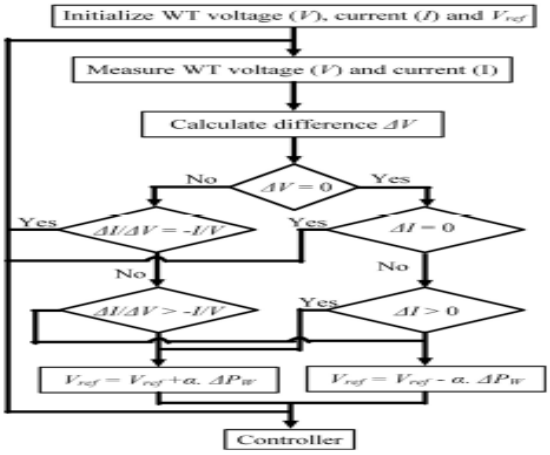

FIGURE 3. MPPT algorithm of the wind system

As shown in Figs. 4 and 5, the PV conversion system can also be operated under MPPT for maximum power extraction or off-MPPT for power balance depending on the state of the storage system. Additionally, in the event that there is excess power generation but insufficient battery capacity, in order to lower the generated power and keep the power balanced in the standalone system, the proposed energy management system switches the PV controller from the MPPT mode to the off-MPPT mode. The voltage reference in off-MPPT is implemented as

$$V_{ref} = \frac{P_L - P_{PV}}{I_{PV}} \text{(9)}$$

Where Ppv is the power from the PV panel energy system and PL is the load power.

C. Modelling of the Battery System:

In this application, the DC-link of the microgrid is connected to a standard battery via a bidirectional DC-DC back-boost converter (see Figure 6). This converter's job is to keep the DC-link voltage constant regardless of source and load power variations.

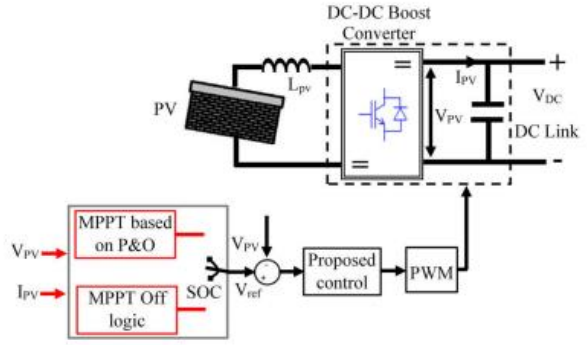

FIGURE 4. Solar energy system with controller

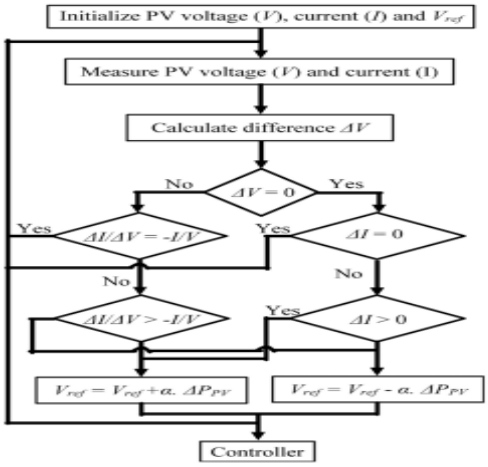

FIGURE 5. MPPT algorithm of the solar energy system.

In order to calculate the battery's reference current and design the voltage controller using the suggested strategy, the DC-link voltage is regulated at its references as shown in Fig. 6. The following describes how the Battery State of Charge (SOC) model is modelled.

$$SOC = 100\left(1 + \frac{\int I_{bat}\,dt}{Q}\right) \quad (10)$$

Controlling the SOC, or the amount of electricity stored during the charge, is a crucial aspect. The proposed supervisory system must be able to detect the battery SOC in order to take action based on its condition and the required power. The ampere-hours stored in a battery over a period of time t correspond to a nominal capacity Q and a charging current Ibat. Battery charge-discharge is influenced by demand, available power, and SOC. Based on the SOC limits, the battery's energy limitations are established:

$$SOC_{min} \leq SOC \leq SOC_{max} \quad (11)$$

Where SOCmin and SOCmax represent the lowest and highest permissible states for battery safety.According to the specifications of the battery storage system, the maximum power permitted during the charge/discharge of the battery system is fixed at 6525 Watts during the charge phase and at 10440 Watts during the discharge phase.

D. Modelling of AC Grid:

A buck-to-buck converter is employed, which is used for both wind and AC grid conversion (see Figure 7).

FIGURE 6. AC load system.

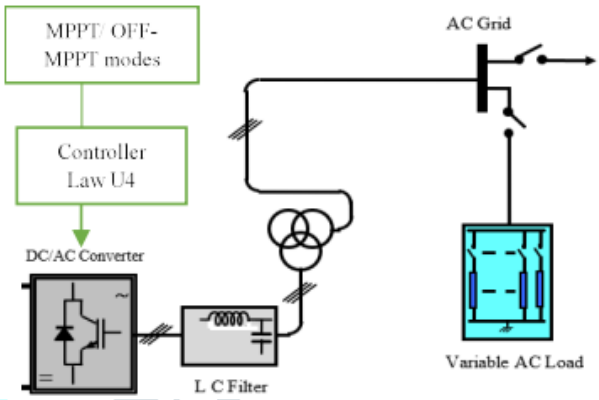

The AC grid converter system's mathematical modelling can then be expressed as follows:

$$\frac{dV_g}{dt} = \frac{I_g}{C_g} - \frac{I_{Lg}}{C_g} \quad (12)$$

Where Ig represents the rectified grid current and Vg represents the rectified grid voltage input to the boost converter.

E. Modelling of the Load side converter:

As seen in Figure 1, the DC priority loads are connected using a parallel DC-DC buck converter because their power loads are constant. These parallel converters are used to distribute the load and reduce stress on the converters.

$$\frac{U_p V_{dc}}{L_p} = \frac{dI_{Lp}}{dt} + \frac{V_{LOadp}}{L_p} - D_{ILp} \quad (13)$$

$$\frac{dV_{LOadp}}{dt} = \frac{I_{Lp}}{C_{Lp}} - \frac{V_{LOadp}}{R_{Lp}C_c} + Dv_{Loadp} \quad (14)$$

Where Up stands for the control law, LLp for the inductor's current, VLoadp for the load voltage, DVLoadp for the voltage's dynamic uncertainty, and DILp for the current's dynamic uncertain.

III. Designing of the Controllers:

The generalized model (24)–(26) represented by Ui and the generalized model (27)–(28) represented by Up, respectively, are used to compute the SCCs controller law and the LSCs controller law, respectively, using the proposed intelligent fractional-PID order.The proposed IFO-PID must be designed in two steps: first, the FO-PID must calculate the controller laws, and then the Fuzzy Gain Supervisor must adopt the fixed gains, making the proposed controller adaptive and resilient to parameter uncertainties.To calculate the controllers of the source-side converters and load-side converters, a proportional-integral (PI) control is suggested. Fixed gains, however, are notoriously challenging to compute when parameter uncertainties or variations exist. As a result, the IFO-PID controller is introduced to increase the robustness and address the issues PI loops face.

A. Designing of SSCs Controller:

The SSCs controller law Ui is calculated using the following Lyapunov function:

$$V_{j1} = 0.5e_j^2 \quad (15)$$

Where, $e_j = C_j(V_j - V_j^*)$is the voltage error and V_j^* denotes the desired voltage controller, derivative of e_j it yields:

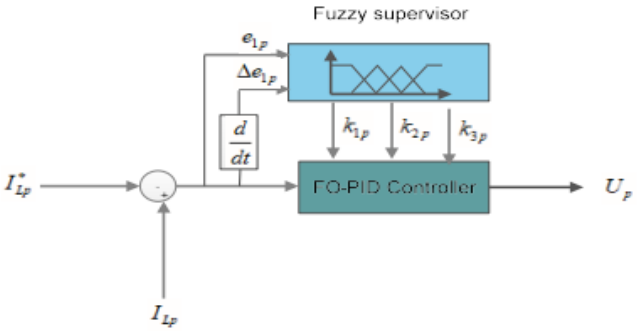

FIGURE 7. SSCs controller law computation with the IFO-PID

The energy management unit creates the desired current for the BSS. As shown in Fig. 8, the fractional order-PID (FO-PID) control is used to design the controller law Ui.

$$e_j = I_j - I_{Lj} - C_j V_j^* \quad (16)$$

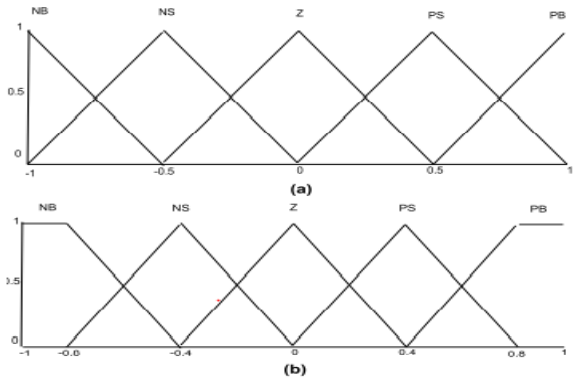

FIGURE 8. The fuzzy controller configuration. (a) Input membership function, (b) Output membership function

Moreover, as was already mentioned, fixed gains are extremely susceptible to changes in parameters. As a result, the fuzzy method is chosen because it solves the problem brought on by imprecise parameters. Fuzzy supervisor is used for the adaptation of gains. According to Lee and Takagi and the method for partitioning these functions is provided. Their approach is predicated on the notion that multiple membership functions can share a single parameter. The benefit of this approach is that the membership functions' parameter count is drastically decreased. The Centre of gravity defuzzification method is used to calculate the crisp outputs, and a Max-Min fuzzy inference is used to obtain the decision-making output. Negative Big (NB), Negative Small (NS), Zero (Z), Positive Big (PB), and Positive Small (PS) are the linguistic variables in Table 1 that correspond to the inputs-outputs of the fuzzy gain scheduling.

TABLE 1. Fuzzy logic rules of the SSCs and LSCs.

$\Delta e_{j,p}$ / $e_{j,p}$	NB	NS	Z	PS	PB
NB	NB	NB	NS	NS	Z
NS	NB	NB	NS	Z	PS
Z	NS	NS	Z	PS	PS
PS	NS	Z	PS	PB	PB
PB	Z	PS	PS	PB	PB

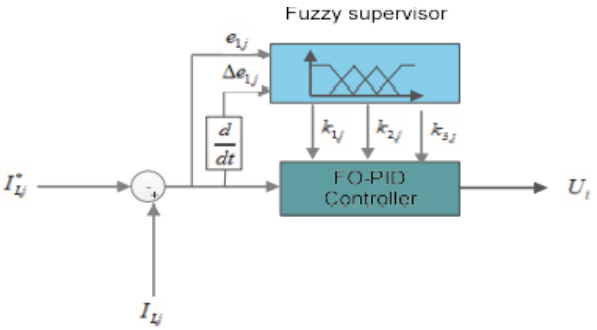

FIGURE 9. SSCs controller law computation with the IFO-PID.

B. Designing of LSCs Controller:

The controller law Up is expressed as follows (see Fig. 10):

$$U_p = k_{1p}e_{1p} + k_{2p}e_{1p}D_t^{-\alpha} + k_{3p}e_{1p}D_t^{-\beta} \quad (17)$$

Where e1p stands for the current error and k1p, k2p, and k3p stand for the gain matrix.

$$e_{1p} = I_{Lp} - I_{Lp}^* \quad (18)$$

C. Energy Managing Unit:

The primary objective of the energy management unit is to coordinate and manage every aspect of the microgrid system. The references of the SSCs and load-side converters controller law are generated by the energy management unit as described by the MPPT Mode/of-MPPT mode algorithm, as can be seen in Figs. 2–7. Based on the measured input power that is both available and consumed for both SSCs and LSCs, the energy management unit generates the references. As previously mentioned, the loads are prioritized to use renewable sources.The BSS controls the DC-link voltage at its reference value while operating in charge/discharge mode. Under various power generation scenarios, including those involving renewable resources and load demand, the power in the microgrid is balanced. The battery storage system is charged using the supply power when the source-side converters produce a lot of energy. The power in the AC grid is used to power the loads as depicted in Fig. 1 in the event that the power produced by the source-side converters is insufficient. The power balance mathematical model is presented as

$$P_W + P_{PV} + P_g = P_{Load} + P_{Battery} \quad (19)$$

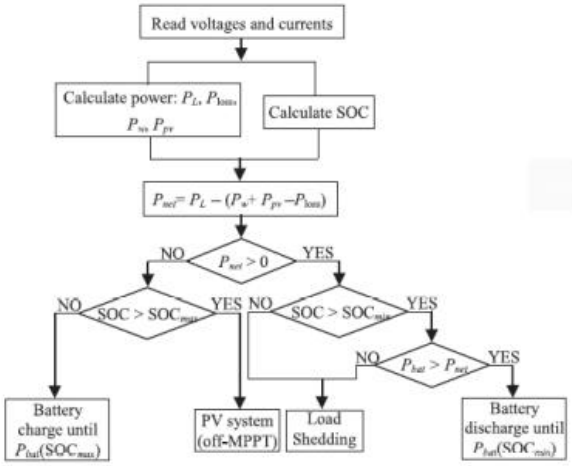

FIGURE 10. Flowchart of Energy management system

The energy management unit has four distinct modes, each of which is dependent on the battery state and generated power, as shown in Fig. 11. The additional power is transferred to charge the battery to its SOCmax when the amount of power generated from renewable sources exceeds the load demand. At this point, the MPPT is turned off. If the generated power is insufficient to supply the load demand, the necessary power is provided by the battery storage system up until SOCmin. If the power generated by the source-side converters is insufficient, the loads are powered by the AC grid.

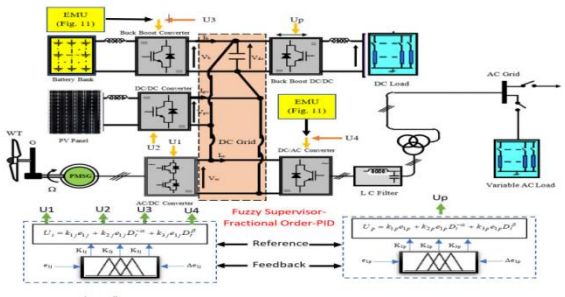

Figure 11: Controlling structure of the proposed system

Fig. 11 depicts the generalized energy management controller structure.

IV. Proposed Fault Injected System:

The defect in the power system that causes the current to deviate from its intended course is referred to as a fault in the power system. The abnormal condition caused by the fault weakens the insulation between the conductors. The system sustains excessive damage as a result of the reduction in insulation. Generally speaking, there are two main categories of power system faults namely open circuit fault and short circuit fault.

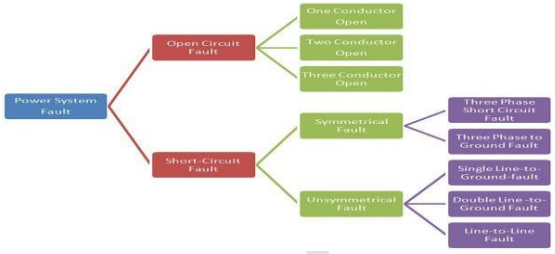

Figure 12: Different types of faults occurred in the system

In this work LLG short circuit fault is implemented at the grid side to obtain the performance of the system with and without fault injected system.

V. RESULTS AND DISCUSSION:

Three main components are shown in the proposed grid-connected hybrid energy system with three phases to ground fault: the BSS connected to the DC-link through its converters; the wind and solar energy sources; and the combined hybrid energy sources. The second element in the case of a smart university represents the workloads deemed to be of the utmost importance. An algorithm for tracking the maximum power point is used to force wind and solar (PV) conversion systems to operate at their highest power.

CASE-1. STEP CHANGE IN WIND SPEED UNDER NORMAL OPERATING CONDITIONS WITHOUT GRID:

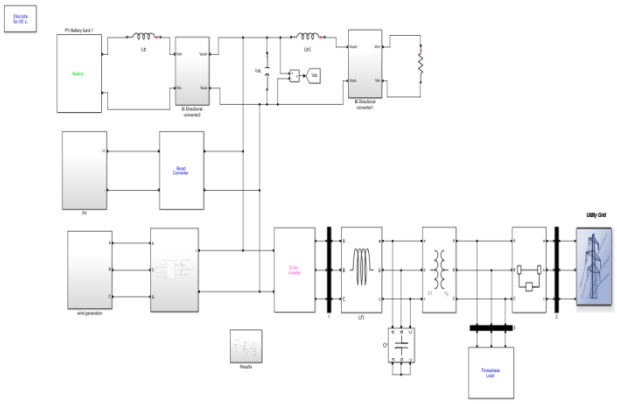

Figure 13: Simulink model grid connected Hybrid system

The above figure-13 will depicts about the simulink model related to case-1 scenario and the related results are shown below**.**

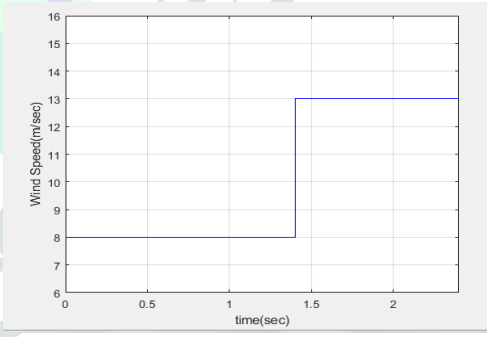

Fig 14: Wind speed.

Fig. 14, shows the wind profile between 8-13m/s. wind speed is varied at 1.4sec from 8 m/s to 13 m/sec.

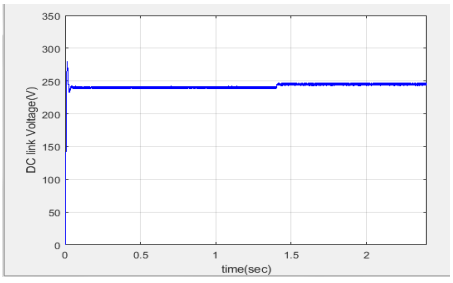

Fig 15: DC-link voltage.

The DC-link voltage of both the SSCs and LSCs for the PI and proposed IFO-PID is shown in Fig. 15, demonstrating that both regulate the DC-link at its reference value. The proposed IFO-PID, on the other hand, outperforms the competition in terms of steady-state error and convergence criterion.

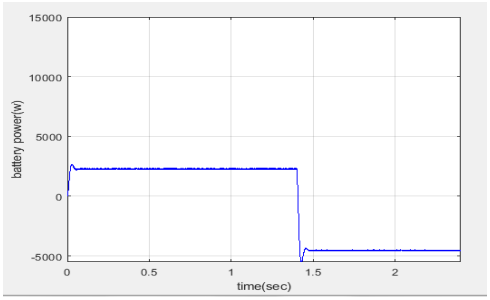

Fig 16: Battery Power

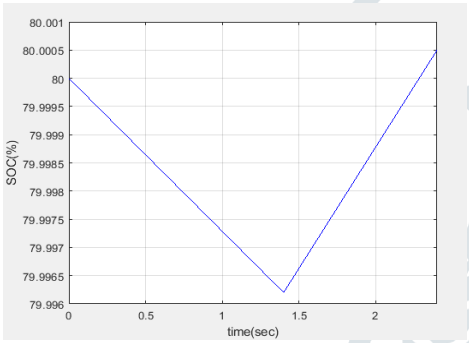

Fig 17: The battery SOC.

The battery power and SOC are shown in Figures 16 and 17. The battery feeds the microgrid with roughly 2300 watts in the time intervals [0-1.4] s when SOC > 20%, while the generated Pdg is greater than the load power in the time intervals [1.4-2.3] s. As a result, the microgrid charges the battery with around 4500 watts.

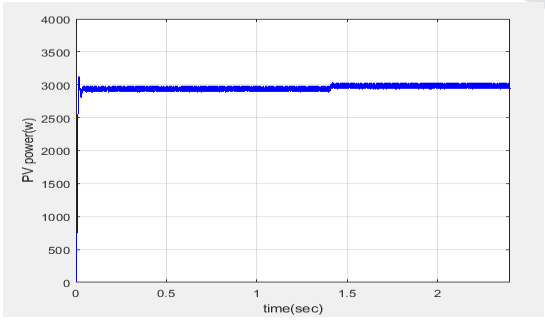

Fig 18: PV power

The generated wind power (shown in Fig. 19) varies between 4000 and 10000 watts depending on the wind speed. Under a brightness of 600 watts/m2 and a temperature of 25 C, a 3000 watts PV power is generated, as shown in Fig. 18

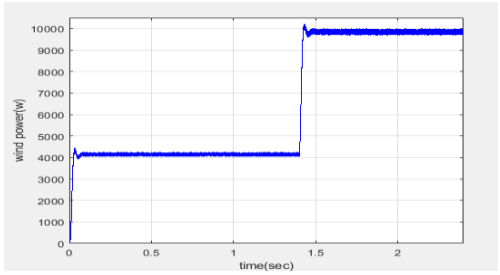

Fig 19: Wind power

The above figure will depict the generated power Pdg from both PV and wind sources. According to the present response, the generated power Pdg varies between 7000 and 13000 watts.

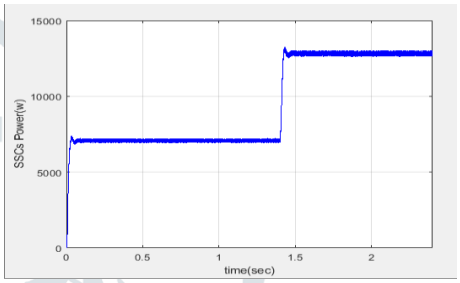

Fig. 20: SSCs power.

The proposed energy management control, as shown in Fig. 20, transfers a constant power to the loads of roughly 8300 watts. The suggested IFO-PID regulates the load output voltage at its reference, as shown in Fig. 21 & 22. (220V).

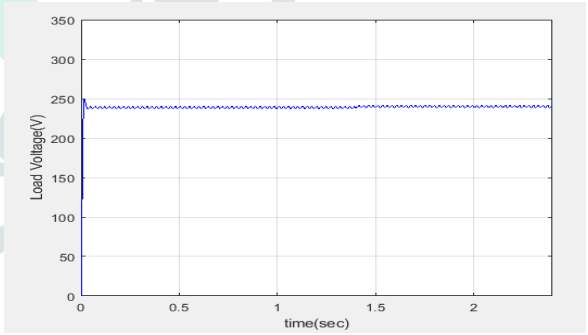

Fig 21: Load Voltage

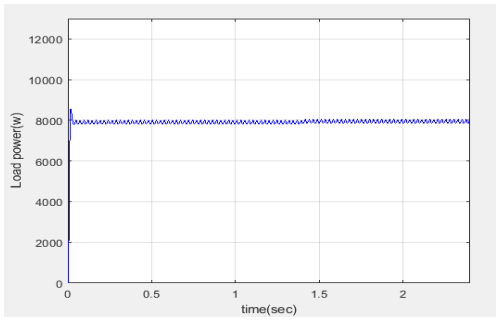

Fig 22: Load power.

CASE-2: RANDOM VARIATIONS IN WIND SPEED UNDER NORMAL OPERATING CONDITIONS WITHOUT GRID

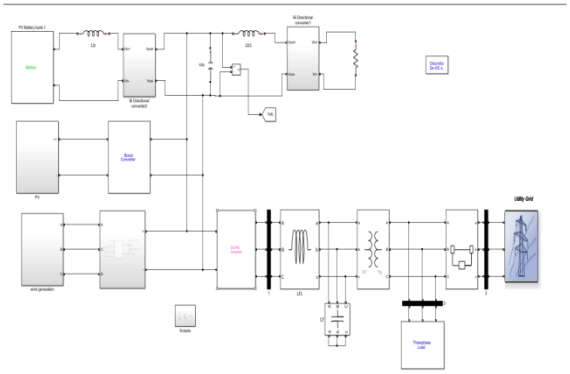

Figure 23: Simulink model grid connected Hybrid system

The above figure-23 will depicts about the simulink model related to case-2 scenario and the related results are shown below**.**A random fluctuation in wind speed and solar radiance is utilized to assess the robustness of the suggested energy management system, as shown in Figures 24 and 25.

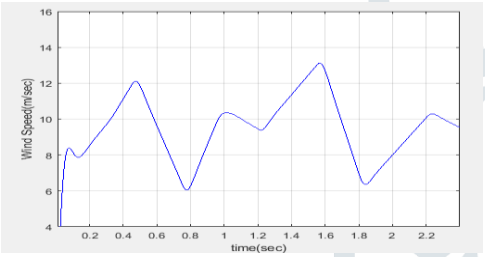

Fig 24: Random wind speed.

The wind power generated under a random wind profile is shown in Figure 24. Based on the given data, the wind system appears to work at MPPT.

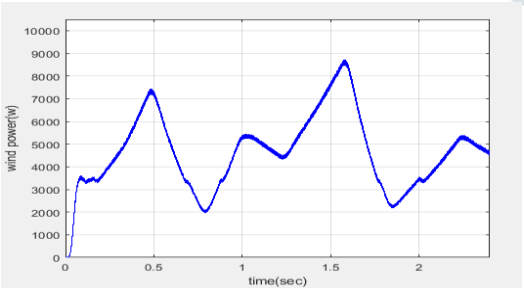

Fig 25: Wind power under random wind speed.

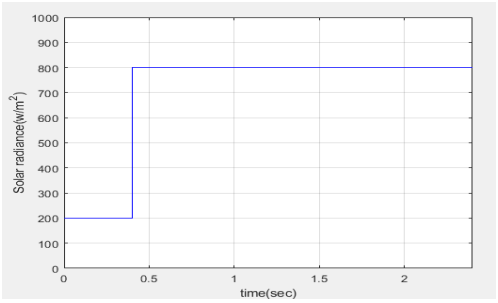

Fig 26: Solar radiance.

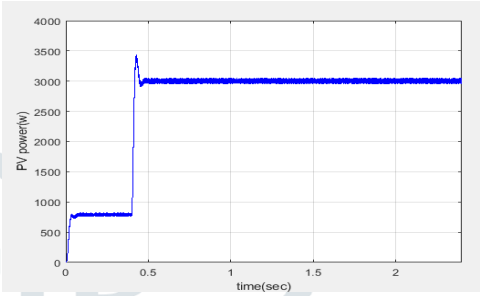

Fig 27: Solar power under random solar radiance.

The solar power generation under a step change in sun irradiation is shown in Figure 26. The radiation is changed from 200 to 800 at 0.4 sec. Figure 27 depicts the highest power extracted from solar.

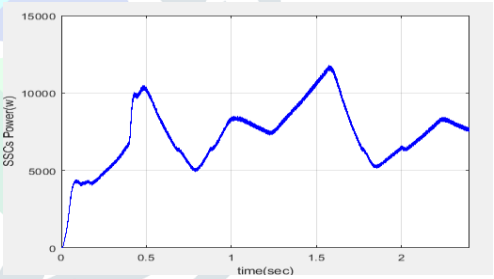

Fig 28: SSCs power under random variations.

Fig. 28 shows the power generated from both PV and wind sources. It can be seen that the power generated is maintained between 5000-13000W.

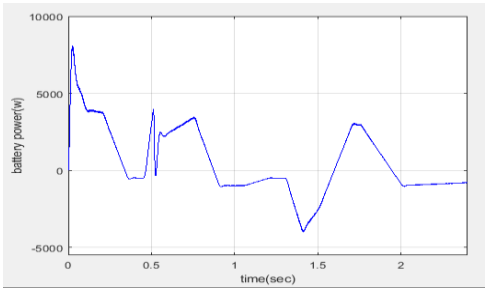

Fig 29: BSS power under random variations.

Figure 29 depicts the BSS power under random wind changes and a step shift in solar, which ranges from 5000

to -5000W. In charge/discharge mode, the BSS performs flawlessly.

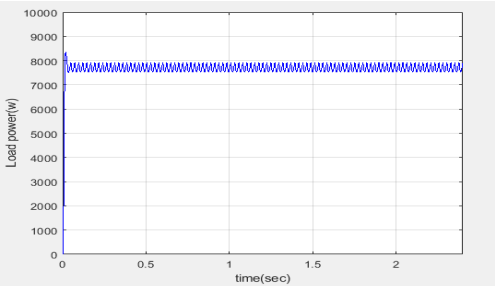

Fig 30: Load power under random variations.

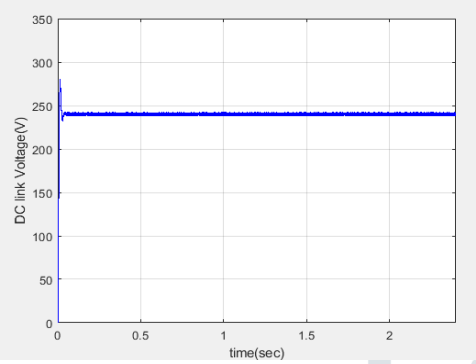

Fig 31: DC-link voltage under random variations

The load power of a DC microgrid is shown in Figure 30. The proposed energy management control, as shown in fig. 11, transfers a constant power to the load of roughly 8300W. The DC-link voltage response is shown in Figure 31. The proposed technique effectively regulates the DC voltage at its reference, as evidenced by the observed response. We can see from the above findings that the energy management system maintains power supply to the loads despite normal and random variations in generation.

CASE-3: GRID CONNECTED HYBRID ENERGY STORAGE SYSTEM UNDER SINGLE PHASE TO GROUND FAULT CONDITION:

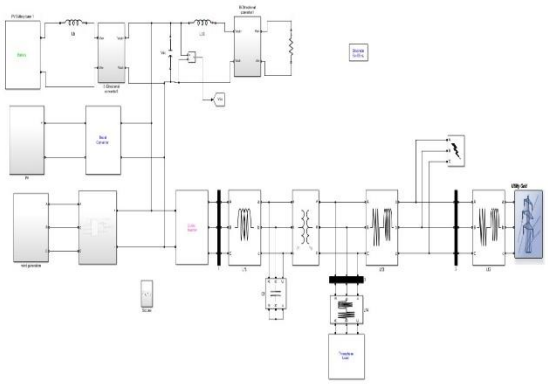

Figure 32: Simulink model of grid connected Hybrid system under single phase to ground fault condition

The above figure will depicts about the simulink model related to case-3 and this related results are shown below.

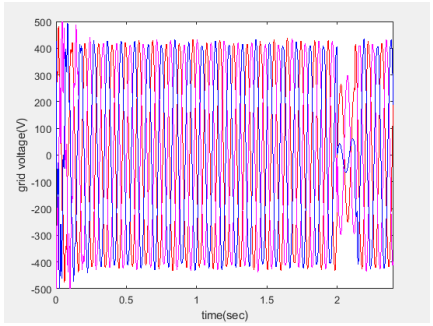

Fig 33: grid voltage

The grid voltage during single phase to ground fault is shown in Figure 33. The fault occurs in the grid between 2 and 2.1 seconds. The grid voltage dropped from 415 to 300 volts during fault timing, yet the generation remained steady. There are no generational differences. That finding was already discussed in the preceding section.

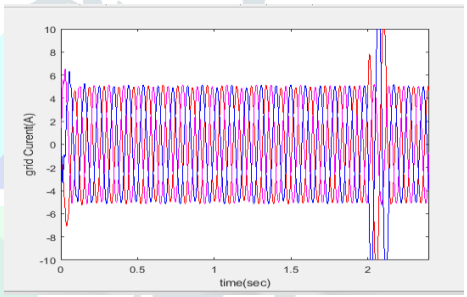

Fig 34: grid current

The grid current under single phase to ground fault is shown in Figure 34. The fault occurs in the grid between 2 and 2.1 seconds, and the grid current is increased from 5 to 10 amps at fault timing.

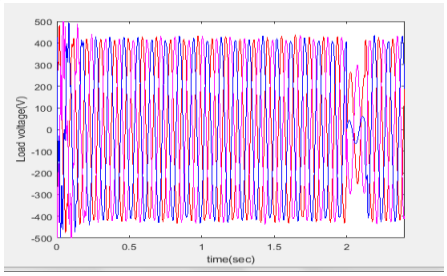

Fig 35: load voltage

The load voltage during single phase to ground fault is shown in Figure 35. The issue occurs in load between 2 and 2.1 seconds. The load voltage is reduced from 415v to 300v during fault timing. The same grid voltage is being transferred to the load here.

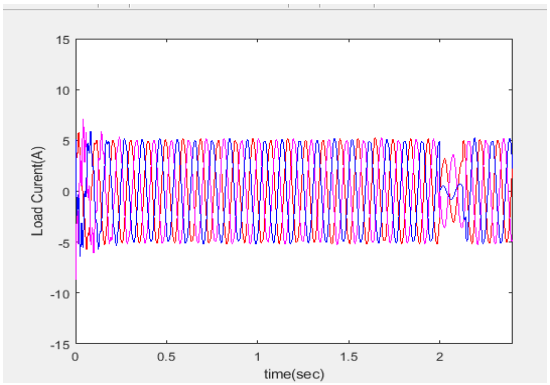

Fig 36: load current

Fig 36 shows the load current under single phase to ground fault. The fault is occurred in grid from 2sec to 2.1sec, at fault timing the grid current is decreased from 5A to 4A.

CASE- 4: GRID CONNECTED HYBRID ENERGY STORAGE SYSTEM UNDER THREE PHASE TO GROUND FAULT CONDITION

Figure 37: Simulink model of grid connected three phase to ground fault condition phase to ground fault condition

The grid voltage during three phase to ground fault is shown in Figure 37. The fault occurred in the grid between 2 and 2.1 seconds. The grid voltage dropped from 415 to 50 volts during fault timing, yet the generation remained steady. There are no generational differences. In the preceding part, we discussed the outcomes.

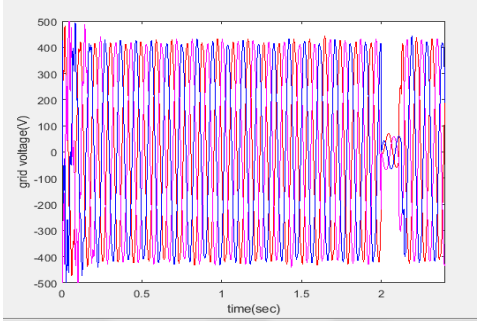

Fig 38: grid voltage

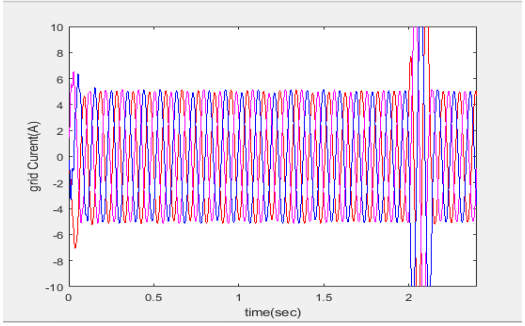

Fig 39: Grid current

Fig 39 shows the grid current under three phase to ground fault. The fault is occurred in grid from 2sec to 2.1sec, at fault timing the grid current is increased from 5A to 10A

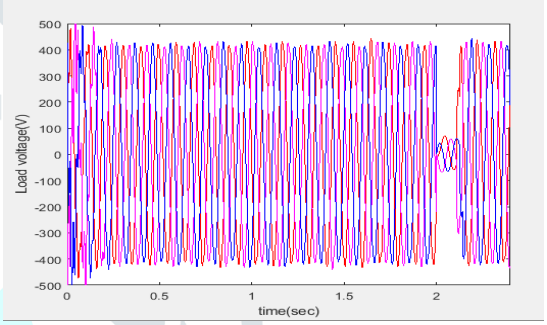

Fig 40: Load voltage

The grid voltage during three phase to ground fault is shown in Figure 40. The fault happened between 2 and 2.1 seconds of load. The load voltage is reduced from 415v to 50v during fault timing. The same grid voltage is being transferred to the load here.

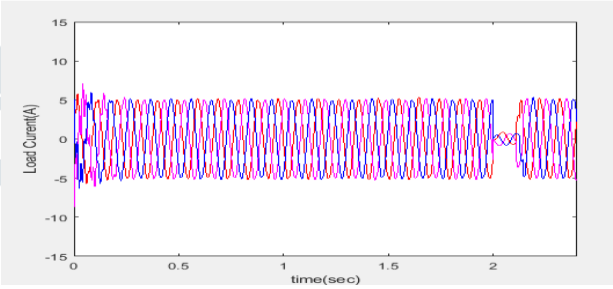

Fig 41: load current

The load current under three phase to ground fault is shown in Figure 41. The fault occurs in the grid between 2 and 2.1 seconds, and the grid current is reduced from 5 to 1 amps at fault timing.

VI. CONCLUSION:

In this study, a novel combined fuzzy logic and fractional-order proportional-integral-derivative (FO-PID) controller for energy management of hybrid energy sources connected to a smart grid via a DC-interface voltage is proposed. Among the hybrid energy sources coordinated to the DC-microgrid are a battery bank, wind energy, and a photovoltaic (PV) energy source. The source side converters (SCCs) are regulated by the new intelligent fractional order PID system to maximize power removal from renewable energy sources (wind and PV) and enhance the quality of the power supplied to the DC-microgrid. In order to make the microgrid as economical as possible, the (Wind and PV) energy sources are prioritized. The proposed regulator guarantees reliability of service and power. Using the results of Matlab/Simulink simulations, the proposed control design is presented and contrasted with alternative nonlinear controls. According to a broad similar investigation with very twisted fractional order control, FO-PID, and PID, the proposed technique develops more power and exhibits elite execution over the proposed control approaches. Investigations were done on the simulation outcomes for symmetrical and asymmetrical grid faults.

VII. ACKNOWLEDGMENT

I greatly Indebted for forever to my Guide, to my HOD K .Chandra Obula Reddy and all teaching and non-teaching staff who supported directly and indirectly to complete my work. I sincerely thankful to my principal Dr. S.K. Biradar for continue encouragement and active interest in my progress throughout the work. I am grateful being a M.tech Electrical Power System student of Matsyodari Shikshan Sanstha's College of Engineering and Technology, Jalna, Maharashtra.

VII. REFERENCES:

[1] H. T. Dinh, J. Yun, D. M. Kim, K. Lee, and D. Kim, ''A home energy management system with renewable energy and energy storage utilizing main grid and electricity selling,'' IEEE Access, vol. 8, pp. 49436–49450, 2020.

[2] C. Byers and A. Botterud, ''Additional capacity value from synergy of variable renewable energy and energy storage,'' IEEE Trans. Sustain. Energy, vol. 11, no. 2, pp. 1106–1109, Apr. 2020.

[3] M. Rizwan, L. Hong, W. Muhammad, S. W. Azeem, and Y. Li, ''Hybrid Harris Hawks optimizer for integration of renewable energy sources considering stochastic behavior of energy sources,'' Int. Trans. Elect. Energy Syst., vol. 31, no. 2, 2021, Art. no. e12694, doi: 10.1002/2050- 7038.12694.

[4] Y. Sun, Z. Zhao, M. Yang, D. Jia, W. Pei, and B. Xu, ''Overview of energy storage in renewable energy power fluctuation mitigation,'' CSEE J. Power Energy Syst., vol. 6, no. 1, pp. 160–173, 2020.

[5] T. Salameh, M. A. Abdelkareem, A. G. Olabi, E. T. Sayed, M. Al-Chaderchi, and H. Rezk, ''Integrated standalone hybrid solar PV, fuel cell and diesel generator power system for battery or supercapacitor storage systems in khorfakkan, united arab emirates,'' Int. J. Hydrogen Energy, vol. 46, no. 8, pp. 6014–6027, Jan. 2021.

[6] M. Çolak and Ä. Kaya, ''Multi-criteria evaluation of energy storage technologies based on hesitant fuzzy information: A case study for turkey,'' J. Energy Storage, vol. 28, Apr. 2020, Art. no. 101211. [

7] M. A. Hannan, M. M. Hoque, A. Mohamed, and A. Ayob, ''Review of energy storage systems for electric vehicle applications: Issues and challenges,'' Renew. Sustain. Energy Rev., vol. 69, pp. 771–789, Mar. 2017.

[8] R. Amirante, E. Cassone, E. Distaso, and P. Tamburrano, ''Overview on recent developments in energy storage: Mechanical, electrochemical and hydrogen technologies,'' Energy Convers. Manage., vol. 132, pp. 372–387, Jan. 2017.

[9] T. Ma, H. Yang, and L. Lu, ''Development of hybrid battery–supercapacitor energy storage for remote area renewable energy systems,'' Appl. Energy, vol. 153, pp. 56–62, Sep. 2015.

[10] X. Wang, D. Yu, S. Le Blond, Z. Zhao, and P. Wilson, ''A novel controller of a battery-supercapacitor hybrid energy storage system for domestic applications,'' Energy Buildings, vol. 141, pp. 167–174, Apr. 2017.

[11] A. Kadri, H. Marzougui, A. Aouiti, and F. Bacha, ''Energy management and control strategy for a DFIG wind turbine/fuel cell hybrid system with super capacitor storage system,'' Energy, vol. 192, Feb. 2020, Art. no. 116518. [12] A. K. Barik, D. C. Das, A. Latif, S. M. S. Hussain, and T. S. Ustun, ''Optimal voltage–frequency regulation in distributed sustainable energybased hybrid microgrids with integrated resource planning,'' Energies, vol. 14, no. 10, p. 2735, May 2021, doi: 10.3390/en14102735.

[13] A. K. Barik, S. Jaiswal, and D. C. Das, ''Recent trends and development in hybrid microgrid: A review on energy resource planning and control,'' Int. J. Sustain. Energy, vol. 4, pp. 1–15, Apr. 2021, doi: 10.1080/14786451.2021.1910698.

[14] H. Kakigano, Y. Miura, and T. Ise, ''Distribution voltage control for DC microgrids using fuzzy control and gain-scheduling technique,'' IEEE Trans. Power Electron., vol. 28, no. 5, pp. 2246–2258, May 2013.

[15] D. A. Aviles, J. Pascual, F. Guinjoan, G. G. Gutierrez, R. G. Orguera, J. L. Proano, P. Sanchis, and T. E. Motoasca, ''An energy management system design using fuzzy logic control: Smoothing the grid power

profile of a residential electro-thermal microgrid,'' IEEE Access, vol. 9, pp. 25172–25188, 2021.
[16] M. Kumar, S. C. Srivastava, and S. N. Singh, ''Control strategies of a DC microgrid for grid connected and islanded operations,'' IEEE Trans. Smart Grid, vol. 6, no. 4, pp. 1588–1601, Jul. 2015.